ISSN: 2350-0328

International Journal of Advanced Research in Science, Engineering and Technology

Vol. 7, Issue 10 , October 2020

Microstructure Analysis and Evaluation of Corrosion Resistance of Mg-4Sn and Mg-4Sn-0.5Bi Alloys in 3.5 % NaCl

A. H. Ayoub*, M. E. Moussa, M. A. Shoeib, M. A. Waly, M. H. Ali, G. S. Al-Ganainy

Physics Department, Faculty of Science, Ain Shams University, P.O. 11566, Cairo, Egypt.
Department of Manufacturing Technology, Laboratory of Foundry, Central Metallurgical Research and Development Institute (CMRDI), P.O. 87, Helwan, Egypt.
Department of Metal Technology, Laboratory of Corrosion Control & Surface Protection, Central Metallurgical Research and Development Institute (CMRDI), P.O. 87, Helwan, Egypt.
Department of Manufacturing Technology, Laboratory of Foundry, Central Metallurgical Research and Development Institute (CMRDI), P.O. 87, Helwan, Egypt.
Physics Department, Faculty of Science, Ain Shams University, P.O. 11566, Cairo, Egypt.
Physics Department, Faculty of Science, Ain Shams University, P.O. 11566, Cairo, Egypt.

ABSTRACT: Mg alloys are highly versatile alloys that are used in different engineering applications such as automotive, medical and sacrificial anodes. To develop new low cost magnesium alloys, Mg-4Sn and Mg-4Sn-0.5Bi alloys have been investigated. X-ray diffraction, optical microscopy, and scanning electron microscopy were studied to reveal the microstructure of each alloy. Electrochemical and immersion tests have been studied. Results showed clearly that the addition of Bi to Mg-4Sn alloy increased the corrosion resistance. It was concluded that the improvement of corrosion was resulted due to the evidence of grain refining of Mg- 4Sn-0.5 Bi alloy.

KEY WORDS: Magnesium-Tin alloy, Microstructure, Corrosion, SEM, EIS, PDP.

I. INTRODUCTION

Nowadays enhancing fuel efficiency of road vehicles and reducing their emissions regard as critical challenges; therefore, lightweight metals are becoming gradually more important. Mg is the lightest of all well-known structural metals with high specific strength, high electromagnetic shielding, and good damping capacity, so its alloys are suitable for transportation industry, 3C applications (computers, cell phones, communications), as well as biomedical sector [1-3]. But its usage is restricted due to the limiting strength and poor creep properties.

On the other hand, Mg and its alloys can be used as a sacrificial anode in cathodic protection to protect the underwater structures and also under the soil, but the problem of corrosion is considered a big obstacle. Mg-Sn system is a heat resistant and low price system which provides a great opportunity of developing new high-strength RE-free Mg alloys [4].

Furthermore, Sn has a beneficial effect on corrosion resistance [5]. A lot of research about Mg-Sn system was covered in the literature. **Song** [6] made a modification on AM70 magnesium alloy and found that Sn was preventing the alloy from localized corrosion. **Moon et al.** [7] elucidated that corrosion resistance of pure Mg and Mg-Sn alloy was increased with increasing Sn content. **Zhang et al.** [8] found that simultaneous additions of Sn and Sr elements to Mg-Zr-Ca alloy improve its corrosion resistance**. Radha et al.** [9]concluded that addition of Sn to Mg/HA composite could be refining the grains and enhance the microstructure as well as decrease the rate of corrosion. **Guo at al.** [10] found that Sn could refine the grains of Mg-9li-3Al and impart high strength. **Jian et al.** [3] added Sn to extruded Mg-5Zn-4Al alloy, and grain refinement was achieved. Consequently, several experiments on enhancing Mg-Sn's corrosion properties are worthwhile.

ISSN: 2350-0328

International Journal of Advanced Research in Science, Engineering and Technology

Vol. 7, Issue 10 , October 2020

Among all other alloying elements, Bi which is included in strengtheners elements (Sb, Sn, Bi) could impart a high melting point phase to the Mg matrix and consequently improve its strength [11]. Mg_3Bi_2 is the intermetallic phase that Bi can form with Mg, and it's a thermally stable compound with melting point 821 °C [12, 13]. Effect of Bi on Mg alloys has addressed by some researchers. **Wang et al.** [14] found that adding Bi to the AZ80 alloy has a significant impact on increasing tensile strength and elongation by refining the grains from 408 µm to 331 µm, and also reported that the optimum Bi percentage is 0.5 wt. %.**Bakhsheshi-Rad, H., et al.** [15] found the addition of 0.5 wt. % Bi to Mg-1.2Ca-1Zn alloy decreased the rate of corrosion and 0.5 wt. % Bi is the optimal composition resulting in high resistance to corrosion. Eventually 0.5 wt. % Bi may enhance the morphology of the second phase particles and may exhibit high resistance to corrosion [15, 16].
Therefore, the aim of the current study is to improve the Mg-Sn corrosion properties by adding 0.5 wt. % of Bi.

II. MATERIALSANDMETHODS

A. Experimental procedure

The charge of about 1.5 kg of the examined Mg-4 wt. %Sn alloy without and with 0.5 wt. % Bi used in this analysis was melted with commercial pure Mg (99.8 wt. %), Sn (99.99 wt. %), and Bi (99.99 wt. %) in a graphite crucible put in an electric resistance furnace. The chemical composition of the investigated alloys, determined by X-ray fluorescence (XRF) analyzer (model Axios advanced-PANALYTICAL, The Netherlands) is shown in **Table 1.**

Table 1.Chemical composition of the prepared alloys in wt. %

Alloy code	Mg	Sn	Bi	Fe	Ca	Cu
A (Mg-4Sn)	Bal.	3.91	-	0.015	0.031	0.031
B (Mg-4Sn-0.5Bi)	Bal.	3.86	0.456	0.013	0.03	0.03

Casting process was carried out under a protective gas mixture of tetrafluoroethane (1 vol. %) and carbon dioxide (Bal.) to avoid oxidation. About 90% efficiency of melting and 10% losses during melting were taken into consideration. After the examined alloy was completely melted the slag was extracted to guarantee the cast's cleanliness. After that, the stirring was done for approximately 3 min using a stainless steel rod to ensure homogenization. Finally, at approximately 720 ° C, the melt was poured into a preheated cast iron mold (100 °C) with an outer diameter of 100 mm and an inner diameter of 50 mm and a length of 250 mm [17].

B. Characterization

Disks having thickness 10 mm were cut for microstructure investigations. Then grinding was performed on sandpapers up to 1200 grit. After that, specimens were polished using alumina suspension (particle size 2µm) and distilled water on suiting until a mirror-like surface was achieved. In order toreveal the microstructure nital solution (95 % ethanol and 5 % nitric acid) was used for etching by immersion the samples on it for 40 sec. [18, 19]. Optical microscope (OM) (model OPTIKA M-790, Italy) was used for metallographic observations. X-ray diffraction (XRD) (model X'PERT PRO, The Netherlands) was used to evaluate phases presented using Cu-Kα radiation (Kα=1.54056 Å) in step scan of 2θ from 20° to 80° with a 0.04 ° increase and a 4 ° /min scanning speed. Scanning electron microscope (SEM) (model FEI-Inspection S50, the Netherland) (operated at 20 kV) equipped with an energy dispersive X-ray spectrometer (EDX) was used to get more information about the microstructure and concentration of elements.

C. Corrosion Test

1. Immersion Test Samples were immersed in 3.5 % NaCl solution for 24, 72, and 168 hr. to perform the immersion test. Prior to immersion, samples (20 x 10 x 2 mm) were grounded using emery paper up to 1200 grit, cleaned in an ultrasonic ethanol bath, then rinsed by deionized water and dried. Then, the weight of the samples was measured. After immersion, samples were cleaned by 200 g/l CrO_3 followed by distilled water cleaning, then weight loss of each sample was calculated.

ISSN: 2350-0328

International Journal of Advanced Research in Science, Engineering and Technology

Vol. 7, Issue 10 , October 2020

2. Electrochemical Tests Potentiodynamic polarization (PDP) and electrochemical impedance spectroscopy (EIS) were conducted using a three-electrode cell configured with silver/silver chloride reference electrode (Ag/AgCl), a platinum wire counter electrode, and a test circle exposed an area of 0.385 cm^2 as a working electrode connected to the MetrolmAutolab B.V System (PGSTAT302N Potentiostat/Galvanostat) computer operated. Samples are pre-immersed in a 3.5 % NaCl at 25°C for about 30 min. to achieve steady-state open-circuit potential (OCP). All electrochemical tests were conducted at least three times to confirm reproducibility. EIS was conducted in a range of frequency from 100 kHz to 100 mHz with 10 points per decade and perturbed amplitude of 5 mV. Nova 1.10 and EC-Lab software were used for analysis and fit the data, respectively.

III. RESULT ANDDISCUSSION

A. Characterization of Phases and Microstructure

Fig 1 shows the micrographs of the as-cast Mg-4Sn and as-cast Mg-4Sn-0.5Bi obtained by an optical microscope. Without adding Bi the microstructure reveals a coarse dendritic structure. But after the addition of Bi, a clear mix of fine dendritic and equiaxed structures was presented. The average grain size is 268.8 µm and 74.5 µm for A and B alloys, respectively. In fact, the segregation behavior of alloying elements during non-equilibrium solidification may restrict grain growth and result in a finer grain structure [20, 21].

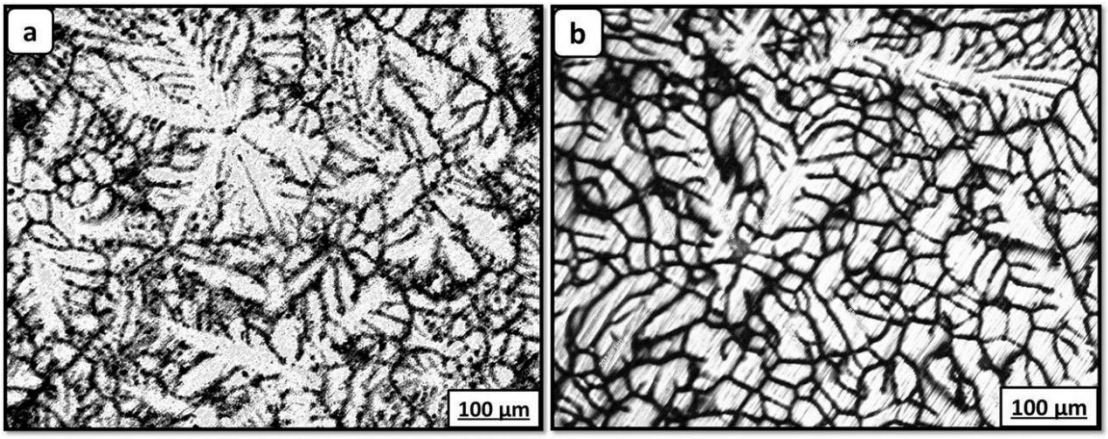

Fig.1Microstructure of a) alloy A and b) alloy B, using optical microscopy.

X-ray diffraction patterns for alloys are given in **Fig. 2**. Each pattern containing the α-Mg phase and Mg_2Sn phase but in alloy B, small peaks of the Mg_3Bi_2 phase were present as well [13, 22].

ISSN: 2350-0328
International Journal of Advanced Research in Science, Engineering and Technology
Vol. 7, Issue 10 , October 2020

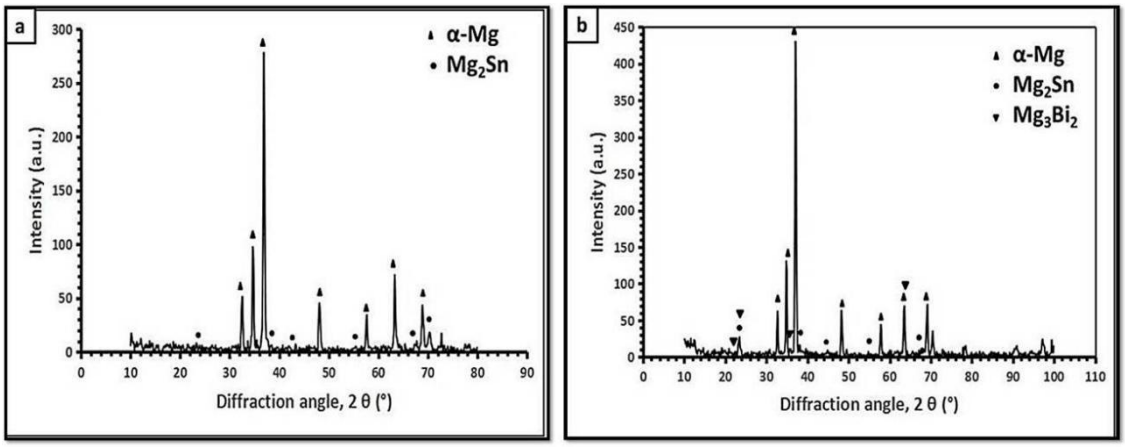

Fig. 2XRD patterns of as-cast a) alloy A and b) alloy B.

Fig.3 shows the SEM images at the same magnification. In alloy A, the microstructure consists of primary α-Mg matrix and Mg_2Sn binary phase presented in the form of spare isolated spherical particles at grain boundaries. In alloy B, a new rod shape Mg_3Bi_2 phase can be detected mainly along the grain boundaries in addition to the existence of α-Mg matrix and Mg_2Sn binary phase which is confirmed by others [13, 22].

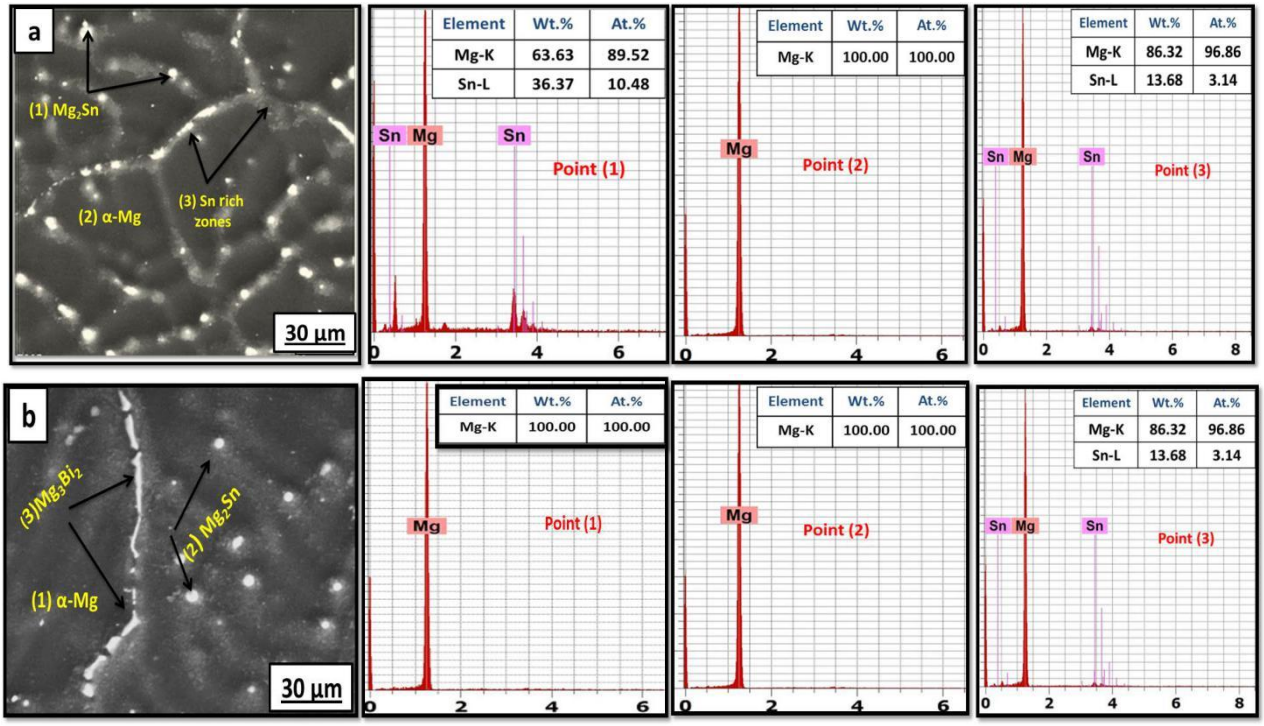

Fig. 3 SEM images with EDX analysis of as-cast a) alloy A and b) alloy B.

Mapping of the existing elements in such alloys is presented in **Fig. 4** where Mg and Sn were the only constituents of alloy A. Sn was found richly at grain boundaries but it also found within the grains. For alloy B, Mg was the main element of the matrix. In addition, Sn was found at grain boundaries, as well as Bi.

ISSN: 2350-0328
International Journal of Advanced Research in Science, Engineering and Technology
Vol. 7, Issue 10 , October 2020

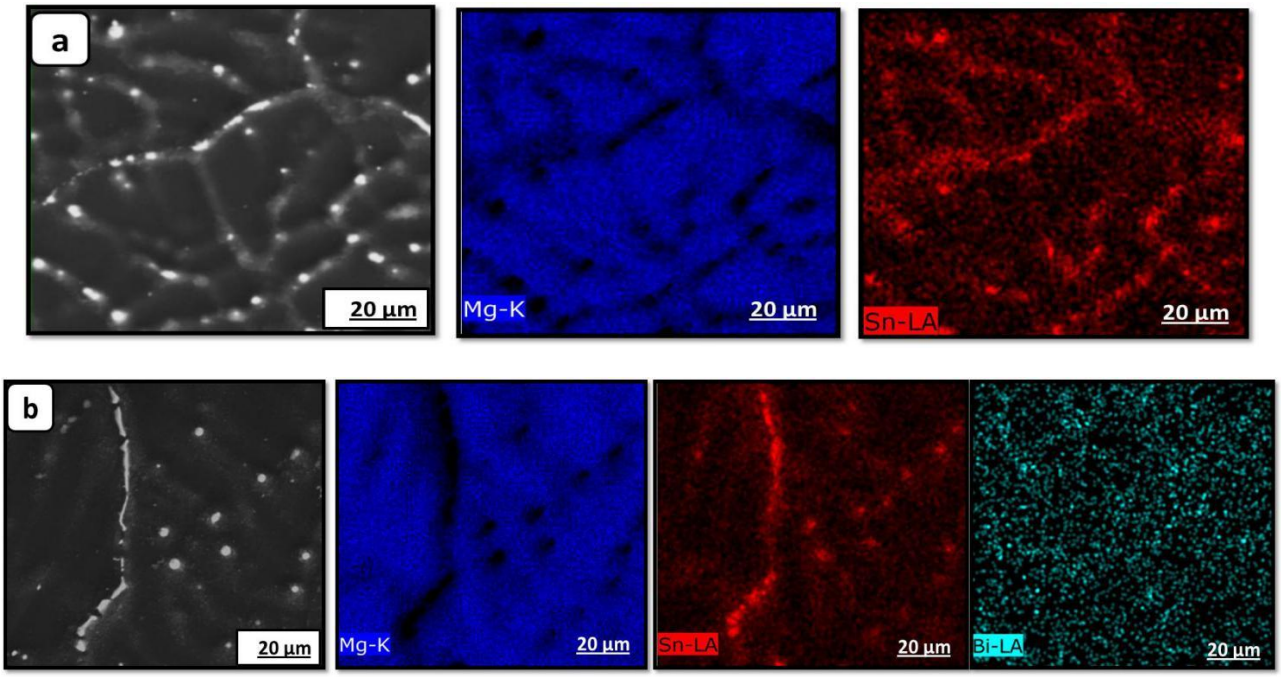

Fig. 4 Elemental mapping of Mg, Sn, and Bi elements in a) alloy A and b) alloy B.

B. Characterization of Corrosion properties

1. Immersion Study:Fig. 5 specifies that the rate of corrosion of these alloys varies over time. It was found that adding Bi lowered the rate of corrosion due to the presence of Mg_3Bi_2 as a second-phase particle as shown by X-ray [16]. Alloy A showed that the corrosion rate decrease with increasing immersion time.

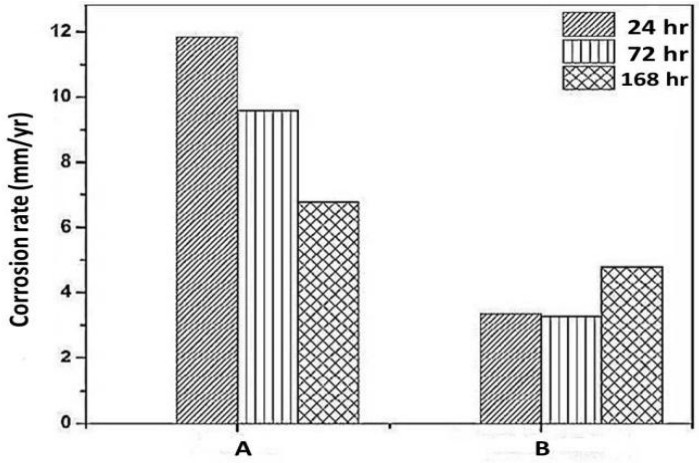

Fig. 5 Corrosion rate for different immersion time for A and B alloys.

This inconsequent result is coincident with publications [23, 24]. The corrosion products could be able to form a thick passive layer on the metal surface with increasing immersion time. This layer protects the metal from excessive corrosion. The corrosion rate of alloy B diminished after 72 hours due to the formation of a passive layer of $Mg(OH)_2$,

ISSN: 2350-0328
International Journal of Advanced Research in Science, Engineering and Technology
Vol. 7, Issue 10 , October 2020

while after 168 hours the corrosion rate rises abruptly due to the breakdown of the passive layer and thus the alloy surface is totally exposed to the solution [16].

2. Electrochemical Tests:PDP curves for A and B alloys are shown in **Fig. 6**. The corrosion potential (E_{corr}), corrosion current density (i_{corr}), polarization resistance (R_p), anodic and cathodicTafel slopes ($\beta a\ \beta c$) and corrosion rate (P_i) obtained from polarization curves via Nova 1.10 software are summarized in **Table 2**. Corrosion rate can be calculated from the following equation [25]:

$Pi \approx 22.85\ icorr$ (1)

And using the following Stearn-Geary relation [25], i_{corr}can be calculated.

$$icorr = \frac{\beta a\ \beta c}{2.3\ (\beta a+\beta c)Rp} \quad (2)$$

It's clear that the potential of alloy B (E_{corr}) was shifted toward positive potentials. Meanwhile, the density of current (i_{corr}) of alloy B (14.328 µA/cm^2) was lower than A (29.085µA/cm^2) whichmeaning that alloy B nobler than A due to the formation of Mg_3Bi_2 particles in Mg matrix [16, 17].Alloy B has a fine grain structure and according ref. [26], the value of (i_{corr}) was affected by the size of grains (gs) and consequently the corrosion rate. The finer grain structure has a higher value of (i_{corr}) and lower value of (P_i).

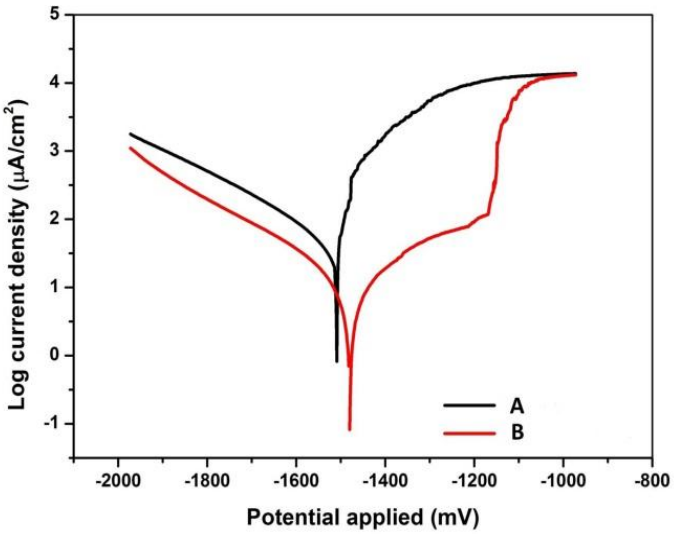

Fig. 6Polarization curves of A and B alloys.

Table 2. Corrosion parameters of A and B alloys.

Alloy	E_{corr} (V)	I_{corr} (µA/cm^2)	β_a (V/decade)	β_c (V/decade)	R_p (kΩ)	Corrosion rate (mm/yr)
A	-1.538	29.085	0.259	-0.0899	1.34075	0.656
B	-1.4702	14.328	0.125	-0.14	3.593	0.323

The EIS spectra in the form of Nyquist plot showed in **Fig. 7** which can be inferred that Mg-4Sn-0.5Bi alloy shows three time constants, one at high frequency (capacitive loop) and it attributed to charge transfer process and surface film formation, another capacitive loop at medium frequency due to mass transport process linked to the adsorption of the monovalent and divalent magnesium ions on the electrode surface, and an onset of a diffusion process at low frequency represents the diffusion of the reactive species able to oscillate and diffuse through the oxide film layer followed by relaxation process [1, 27].

ISSN: 2350-0328

International Journal of Advanced Research in Science, Engineering and Technology

Vol. 7, Issue 10 , October 2020

In order to facilitate the interpretation of EIS data, it can be visualized as an electric equivalent circuit (ECC) representation. ECC is shown in **Fig. 7(b)** R_1 (solution resistance) = 54.5 Ω.cm^2, R_2 (adsorption resistance) = 124 Ω.cm^2, R_3 (surface film resistance) = 36.6 Ω.cm^2, R_4(chargetransfer resistance)= 2220 Ω.cm^2, W(Warburg diffusion element) 2.39 Ω.s^{-1} ,C_1 (double layer of adsorption) = 6.19 x 10^{-9} F/cm^2, *CPE* (capacitance of the surface film) = 8.6 x 10^{-6} F/cm^2, n = 0.68, C_2 (double layer associated with the charge transfer process) = 1.08 x 10^{-6} F/cm^2.

In alloy A, the HF and MF capacitive loops are overlapped to get a large capacitive loop. As well as a large inductive loop was appeared due to the initiation of the formed surface film dissolution and developing some pits (pitting corrosion) [28]. As the radius of the semicircle increase, the resistance to corrosion increased.For alloy A, the equivalent circuit presented in **Fig. 7(a)** was used, where R_1 (solution resistance) = 54.1 Ω.cm^2, R_2(charge transfer resistance)= 1060 Ω.cm^2, R_3 (resistance associated with the inductive element) = 492 Ω.cm^2, *CPE* (constant phase element of the charge transfer process) = 15.7 x 10^{-6} F/cm^2, n = 0.79, L (inductive element) = 134 H. To enhance the fitting quality, *CPE* was used instead of a capacitor because of the inhomogeneity and roughness of the electrode surface.*CPE* is a limiting behavior parameter depending on the varying coefficient n. If n = 1, a pure capacitor exist, if n = 0, a pure resistor exist instead of *CPE* [29].

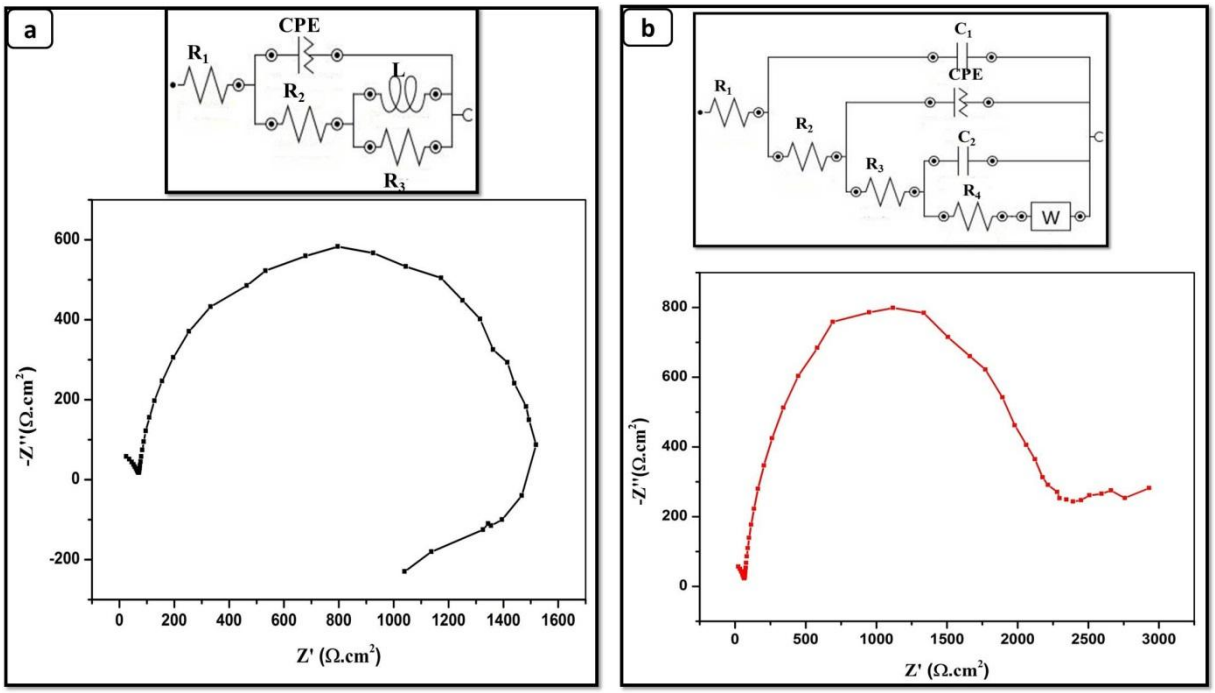

Fig. 7 Nyquist diagram attached with the equivalent circuit for a) alloy A and b) alloy.

As shown in **Fig. 8**, Both Bode plots (impedance and phase) confirmed the Nyquist plot results. For alloy B, the high frequency crest at a phase angle Ø= 60°, corresponding to the capacitive behavior, and the second capacitive loop at medium frequency appeared at Ø = 68°, while at lower frequency the time constant is slightly high and slower electrochemical process occur (diffusion).

For alloy A, one crest corresponding to one capacitive loop, and at low frequency region, the curve goes to positive phase angles which confirm the presence of the inductive loop. Impedance modulus of alloy B is higher than that of alloy A confirming our conclusion about 0.5 wt. % Bi can increase resistance to corrosion.

Immersion test results are coincident with the PDP results in **Fig. 6**. Mg-4Sn curve exhibits a slow increase in anodic current followed by a plateau region corresponding to the formation of a protective oxide layer, but this layer was less adhered at the surface and quickly dissolved. In alloy B, plateau has also appeared which corresponds to the formation of a protective film followed by a sharp increase in current density corresponding to the breakdown of the protective

ISSN: 2350-0328
International Journal of Advanced Research in Science, Engineering and Technology
Vol. 7, Issue 10 , October 2020

film [30]. Although the protective film has been dissolved, the rate of corrosion still lower than alloy A, because of the Mg_3Bi_2 particleslocated at the grain boundaries which act as a corrosion inhibitor discouraging the occurrence of excessive corrosion. Regarding the Nyquist and Bode plots, the diameter of the semicircle and the impedance magnitude of alloy B larger than alloy A, that supports our inference; too, that 0.5 wt. % Bi will increase the resistance to corrosion.

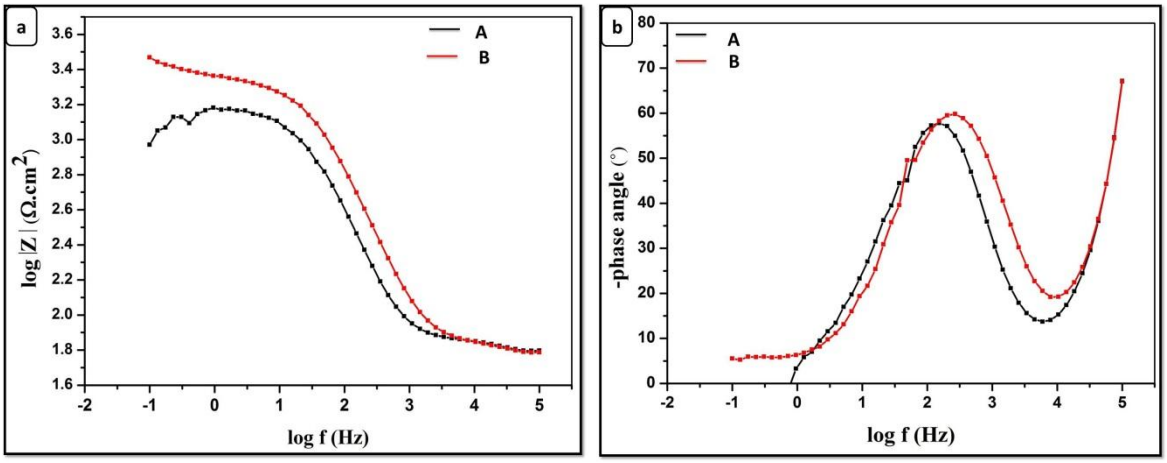

Fig. 8 (a) Bode plots of impedance versus frequency for A and B alloys, (b) Bode plots of phase angle versus frequency for A and B alloys.

C. Microstructure after corrosion

SEM images of the alloys after electrochemical tests in 3.5 % NaCl are shown in **Fig. 9**. It demonstrated that alloy A had plenty of corroded areas and oxide layers on the surface. After adding Bi, the corroded and oxide areas are therefore decreased and a homogenized form of corrosion was obtained. Furthermore, Mg_3Bi_2 particles found richly at grain boundaries inhibiting the corrosion process**.**

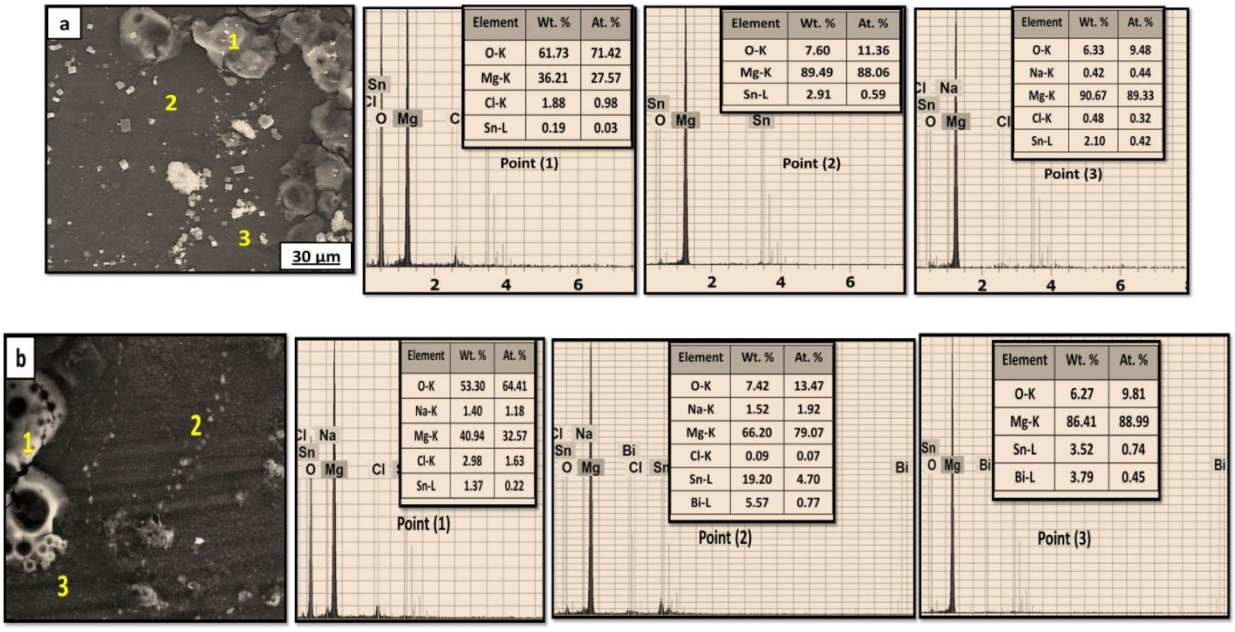

Fig.9 SEM images with EDX analysis of a) A and b) B alloys after polarization in 3.5 % NaCl.

ISSN: 2350-0328
International Journal of Advanced Research in Science, Engineering and Technology
Vol. 7, Issue 10 , October 2020

Elementary study of corroded layers with EDX is shown in **Fig. 10**. In addition to the presence of Mg, Sn, and Bi in the studied alloys, there are exist some new elements after the exposure to the corrosion environment like Cl and O. In alloy A, oxygen has fully covered the surface of the specimen, while in alloy B; the percentage of oxygen and aggressive chloride ions is smaller than the base alloy. It was also observed that, the content of Bi increased after corrosion, evidencing that the corrosion products are formed only from Mg as well as Sn [31].

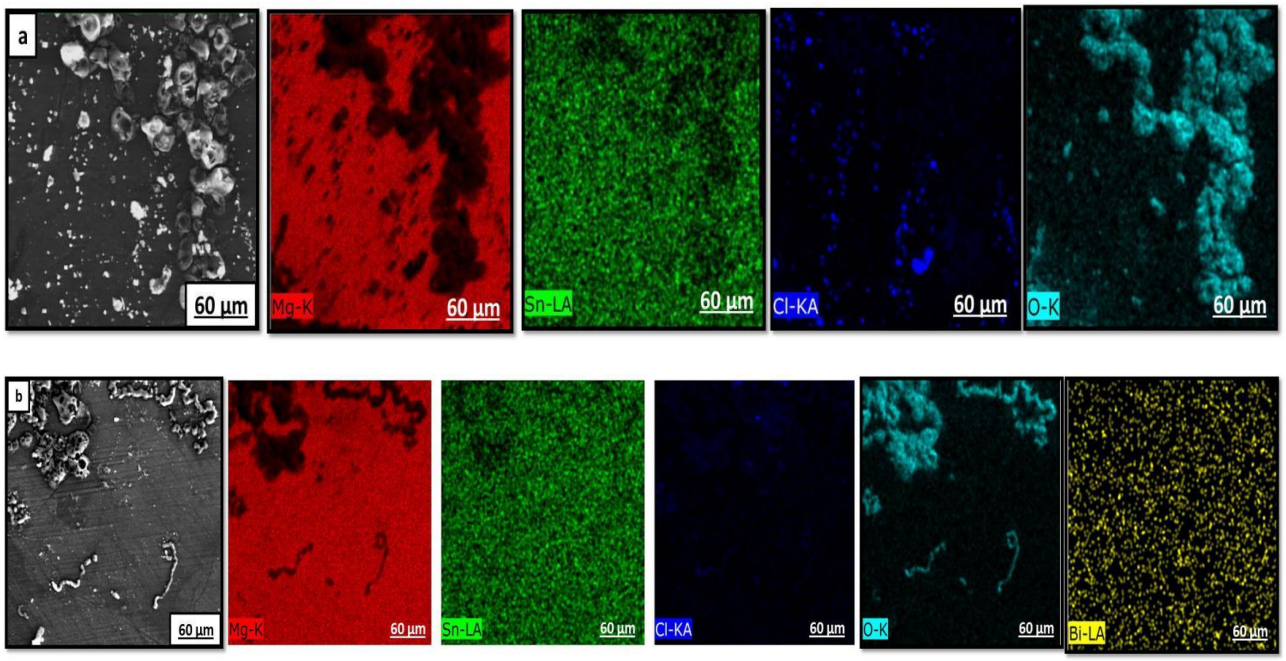

Fig.10 Elemental mapping in a) A and b) B alloys after electrochemical tests.

Fig. 11 shows XRD results of corrosion products formed on the surface after 168 hr. of immersion. The compound $Mg(OH)_2$ was found to be the main corrosion product for both alloys and it can be formed through the following reaction mechanism [32], when Mg immersed in the solution, it dissolves into Mg^{2+}, releasing hydrogen gas and OH^- was resulted as well (equation 3, 4).

Generation of OH^- ions made the solution more alkaline, and then Mg^{2+} can react with OH^- and form the protective layer $Mg(OH)_2$ (equation 5). This layer might be attacked by the aggressive cl^- ions formed $MgCl_2$ layer (equation 6).

$$Mg \longrightarrow Mg^{2+} + 2e^- \quad (3)$$

$$2H_2O + 2e^- \cancel{2O} \rightarrow H^- + H_2 \quad (4)$$

$$Mg^{2+} + 2\,OH^- \longrightarrow Mg(OH)_2 \quad (5)$$

$$Mg(OH)_2 + 2Cl^- \longrightarrow MgCl_2 + 2OH \quad (6)$$

ISSN: 2350-0328
International Journal of Advanced Research in Science, Engineering and Technology
Vol. 7, Issue 10 , October 2020

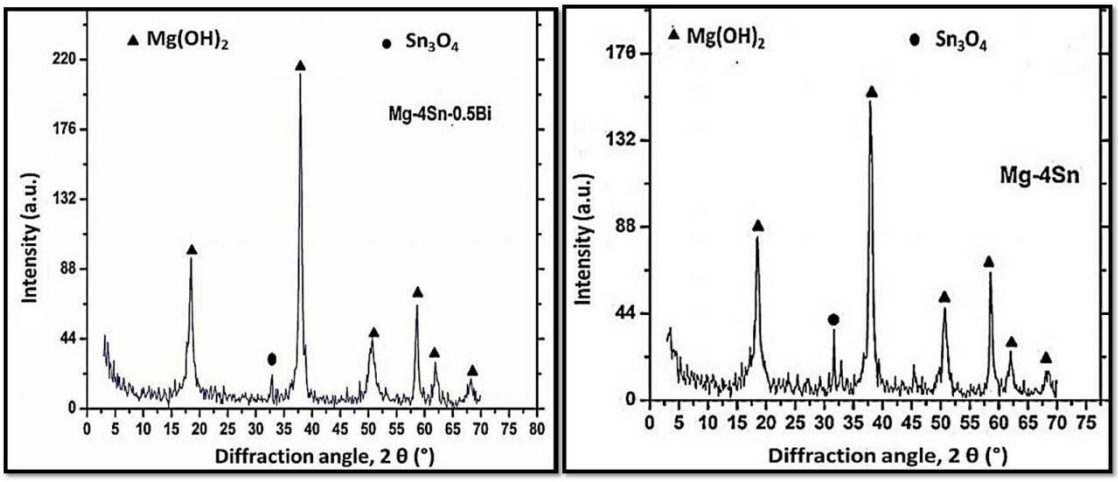

Fig.11 XRD after immersion in 3.5 % NaCl for 168 hours.

IV. CONCLUSION

On the basis of the present study, the following conclusion could be drawn; after the addition of 0.5 wt. % Bi, a fine grain structure was obtained and Mg-4S-0.5Bi alloy has a microstructure of α-Mg matrix and in addition to Mg_2Sn, there exist Mg_3Bi_2 as a second phase.

After exposure of the two alloys to 3.5 % NaCl for 24, 72, and 168 hours, Mg-4Sn-0.5Bi alloy showed a lower weight loss per unit area and consequently lower corrosion rate.

XRD analysis for the corrosion products of 168 hours characterized that $Mg(OH)_2$ layer, and the intensity of $Mg(OH)_2$ peaks was lowered after the addition of 0.5 wt. % Bi, which infer that by excessive immersion (one week or more), the protective layer tends to dissolve and the rate of corrosion becomes high (but it's still less than Mg-4Sn alloy). PDP and EIS spectrum showed that Mg-4Sn-0.5Bi alloy had a nobler corrosion potential, lower corrosion current density, and higher corrosion resistance than Mg-4Sn alloy.

The agreement of the weight loss, PDP, and EIS among these completely different independent methods indicates the validity of the obtained results. Several attempts to detect the effect of different concentrations more than 0.5 wt. % of Bi will be addressed in future work.

REFERENCES

[1]. Chunming Wang, ShuaiGuo, LumingZeng, DesenJianchaoXu, Munan Yang, Tongxiang Liang, "Effects of Second Phases on Microstructure, Microhardness, and Corrosion Behavior of Mg-3Sn-(1Ca) Alloys", Materials, Aug. 2019, pg no: 1-12.
[2]. SebastiánFeliu, Jr."Electrochemical Impedance Spectroscopy for the Measurement of the Corrosion Rate of Magnesium Alloys: Brief Review and Challenges", Metals, Jun. 2020, pg no:1-22.
[3]. Jian Ding, Xin Liu, Yujiang Wang, Wei Huang, Bo Wang, Shicheng Wei, Xingchuan Xia, Yi Liang, Xianhua Chen, Fusheng Pan, BinshiXu, "Effect of Sn addition on microstructure and corrosion behavior of as-extruded Mg–5Zn–4Al alloy", Materials, Jun. 2019, pg no: 1-15.
[4]. B.Q. Shi, R.S. Chen, W. Ke, "Solid solution strengthening in polycrystals of Mg–Sn binary alloys", Journal of Alloys and Compounds, 2011, pg no:3357-3362.
[5]. T. Abu Leil, N. Hort, W. Dietzel, C. Blawert, Y. Huang, K.U. Kainer, K.P. Rao, "Microstructure and corrosion behavior of Mg-Sn-Ca alloys after extrusion", Transaction of Nonferrous Metals, 2009, pg no: 40-44.
[6]. Guang-Ling Song, "Effect of tin modification on corrosion of AM70 magnesium alloy", Corrosion science,2009, pg no: 2063–2070.
[7]. Sungmo Moon, Yunkyung Nam, "Anodic oxidation of Mg–Sn alloys in alkaline solutions", Corrosion Science, 2011, pg no: 494–501.
[8]. Wenjin Zhang, Meiheng Li, Qian Chen, Wangyu Hu, Wenmei Zhang, Wang Xin, "Effects of Sr and Sn on microstructure and corrosion resistance of Mg–Zr–Ca magnesium alloy for biomedical applications", Materials Destination, 2012. Pg no: 379–383.
[9]. R Radha, D. Sreekanth, "Mechanical and corrosion behaviour of hydroxyapatite reinforced Mg-Sn alloy composite by squeeze casting for biomedical applications", Journal of Magnesium and Alloys, 2020, pg no: 452–460.
[10]. J. Guo, L.L. Chang, Y.R. Zhao, Y.P. Jin, "Effect of Sn and Y addition on the microstructural evolution and mechanical properties of hot-extruded Mg-9Li-3Al alloy", Material Characterization, 2019, pg no: 35–42.

ISSN: 2350-0328

International Journal of Advanced Research in Science, Engineering and Technology

Vol. 7, Issue 10 , October 2020

[11]. M. O. Pekguleryuz and M. M. Avedesian, "Magnesium alloying, some potentials for alloy development", Journal of Japanese Institute of Light Metal, 1992, pg no: 679-686.
[12]. HansongXue, Xinyu Li, Weina Zhang, Zhihui Xing, JinsongRao and FuSheng Pan, "Effect of Bi on Microstructure and Mechanical Properties of Extruded AZ80-2Sn Magnesium Alloy", High Temperature Material Processes, 2016, pg no: 97-10.
[13]. M. Keyvani, R. Mahmudi, G. Nayyeri, "Effect of Bi, Sb, and Ca additions on the hot hardness and microstructure of cast Mg–5Sn alloy", Materials Science and Engineering A, 2010, pg no: 7714-7718.
[14]. WANG Ya-xiao, ZHOU Ji-xue, WANG Jie, LUO Tian-jiao, YANG Yuan-sheng, "Effect of Bi addition on microstructures and mechanical properties of AZ80 magnesium alloy", Transaction of Nonferrous Metal Society of China, 2011, pg no: 711-716.
[15]. H.R. Bakhsheshi-Rad, E. Hamzah, H.Y. Tok, M. Kasiri-Asgarani, S. Jabbarzare, and M. Medraj, "Microstructure, In Vitro Corrosion Behavior and Cytotoxicity of Biodegradable Mg-Ca-Zn and Mg-Ca-Zn-Bi Alloys",Journal of Material Engineering and Performance, 2017, pg.no: 653-666.
[16]. M. Y. Tok, E. Hamzah, H. R. Bakhsheshi-Rad, "The role of bismuth on the microstructure and corrosion behavior of ternary Mg–1.2 Ca–xBi alloys for biomedical applications", Journal of Alloys and Compounds, 2015,pg no: 335-346.
[17]. M. E. Moussa, H.I. Mohamed, M. A. Waly, G. S. Al-Ganainy, A. B. Ahmed, "Comparison study of Sn and Bi addition on microstructure and bio-degradation rate of as-cast Mg-4wt% Zn alloy without and with Ca-P coating", Journal of Alloys Compounds, 2019, pg no: 1239-1247.
[18]. G. Nayyeri, R. Mahmudi, F. Salehi, "The microstructure, creep resistance, and high-temperature mechanical properties of Mg-5Sn alloy with Ca and Sb additions, and aging treatment", Materials Science and Engineering A, 2010, pg no: 5353-5359.
[19]. G. Nayyeri, R. Mahmudi, "Enhanced creep properties of a cast Mg–5Sn alloy subjected to aging-treatment", Materials Science and Engineering A, 2010, pg no: 4613-4618.
[20]. H. R. Bakhsheshi-Rad, M. H. Idris, M.R. Abdul Kadir, A. Ourdjini, M. Medraj, M. Daroonparvar, E. Hamzah, "Mechanical and bio-corrosion properties of quaternary Mg–Ca–Mn–Zn alloys compared with binary Mg–Ca alloys", Materials Destination, 2018,pg no: 283-292.
[21]. Y. Ali, D. Qiu, B. Jiang, F. Pan, M. X. Zhang, "Current research progress in grain refinement of cast magnesium alloys: A review article", Journal of Alloys and Compounds, 2015, pg no: 639-651.
[22]. M. Keyvani, R. Mahmudi, G. Nayyeri, "Microstructure and impression creep characteristics of cast Mg-5Sn-xBi magnesium alloys", Metallurgical and Materials Transaction A, 2011,pg no: 1990-2003.
[23]. D. Thirumalaikumarasamy, K. Shanmugam, V. Balasubramanian, "Comparison of the corrosion behaviour of AZ31B magnesium alloy under immersion test and potentiodynamic polarization test in NaCl solution", Journal of Magnesium and Alloys, 2014,pg no: 36-49.
[24]. E.S Sherif, "A comparative study on the electrochemical corrosion behavior of iron and X-65 steel in 4.0 wt% sodium chloride solution after different exposure intervals", Molecules, 2014, pg no: 9962-9974.
[25]. Fuyong Cao, Zhiming Shi, Guang-Ling Song, Ming Liu, Andrej Atren, "Corrosion behaviour in salt spray and in 3.5% NaCl solution saturated with Mg(OH)2 of as-cast and solution heat-treated binary Mg–X alloys: X = Mn, Sn, Ca, Zn, Al, Zr, Si, Sr", Corrosion Science, 2013, pg no: 60-97.
[26]. K. D. Ralston, N. Birbilis, C. H. J. Davies, "Revealing the relationship between grain size and corrosion rate of metals", ScriptaMaterialia, 2010, pg no: 1201-1204.
[27]. NandiniDinodi, A. NityanandaShetty, "Electrochemical investigations on the corrosion behaviour of magnesium alloy ZE41 in a combined medium of chloride and sulphate", Journal of Magnesium and Alloys, 2013, pg no: 201-209.
[28]. Rong-Chang Zeng, Zheng-Zheng Yin, Xiao-Bo Chen, Dao-KuiXu, "Corrosion types of magnesium alloys. Magnesium alloys: selected issue, intech, chapter 3, 2018, pg no: 30-52.
[29]. G. Liu, S. Khorsand, S. Ji, "Electrochemical corrosion behaviour of Sn-Zn-xBi alloys used for miniature detonating cords", Material Science and Technology, 2016,pg no: 1618-1628.
[30]. Jean-Baptiste Jorcin, Mark E. Orazem Nadine Pébère, Bernard Tribollet, "CPE analysis by local electrochemical impedance spectroscopy", Electrochemical Acta, 2006, pg no: 1473-1479.
[31]. Hong Xu , Zhiquan Wu, Xiaoru Wang, Xin Zhang , JipingRen, Yang Shi, Zepu Wang, Liwei Wang, Changhua Liu, "Corrosion mechanism and corrosion model of Mg-Y alloy in NaCl solution", J. Wuhan Uni. Techn. Mater. Sci. Ed., Vol. 31, pp. 1048–1062, 2016.
[32]. H. I. Mohamed, M. E. Moussa, M. A. Waly, G. S. Al-Ganainy, A. B. Ahmed, M. S. Talaat, "Effect of adding Sb on microstructure, mechanical properties and in vitro degradation behavior of as cast Mg-4wt% Zn alloy for medical application", Journal of Surface Engineered Materials and Advanced Technology, 2017, pg no: 69-85.

Name	Affiliation	Country
Asmaa HamedAyoub	Demonstrator Faculty of Science Ain Shams University	Egypt
Mohamed EssaMoussa	Doctor Department of Manufacturing Technology, Laboratory	Egypt

ISSN: 2350-0328
International Journal of Advanced Research in Science, Engineering and Technology
Vol. 7, Issue 10 , October 2020

	of Foundry Central Metallurgical Research and Development Institute	
Madiha Shoeib	Professor Department of Metal Technology, Laboratory of Corrosion Control & Surface Protection Central Metallurgical Research and Development Institute	Egypt
Mohamed Waly	Professor Department of Manufacturing Technology, Laboratory of Foundry Central Metallurgical Research and Development Institute	Egypt
Mohsen Ali	Professor Faculty of Science Ain Shams University	Egypt
Gamila Al-Ganainy	Professor Faculty of Science Ain Shams University	Egypt